time window and a box-shaped time window. Each analysis varies the central time of the window, T_0, and the duration T_W (from seconds to years) of the potential signal to find the four parameters (Φ_{100}, γ, T_0, T_W) that maximize the likelihood ratio, which is defined as the test statistic *TS*. (For the Gaussian time window, T_W represents twice the standard deviation.) The test statistic includes a factor that corrects for the look-elsewhere effect arising from all of the possible time windows that could be chosen (*30*).

For each analysis method (time-integrated and time-dependent), a robust significance estimate is obtained by performing the identical analysis on trials with randomized datasets. These are produced by randomizing the event times and recalculating the RA coordinates within each data-taking period. The resultant *P* value is defined as the fraction of randomized trials yielding a value of *TS* greater than or equal to the one obtained for the actual data.

Because the detector configuration and event selections changed as shown in Table 1, the time-dependent analysis is performed by operating on each data-taking period separately. (A flare that spans a boundary between two periods could be partially detected in either period, but with reduced significance.) An additional look-elsewhere correction then needs to be applied for a result in an individual data segment, given by the ratio of the total 9.5-year observation time to the observation time of that data segment (*30*).

Neutrinos from the direction of TXS 0506+056

The results of the time-dependent analysis performed at the coordinates of TXS 0506+056 are shown in Fig. 1 for each of the six data periods. One of the data periods, IC86b from 2012 to 2015, contains a significant excess, which is identified by both time-window shapes. The excess consists of 13 ± 5 events above the expectation from the atmospheric background. The significance depends on the energies of the events, their proximity to the coordinates of TXS 0506+056, and their clustering in time. This is illustrated in Fig. 2, which shows the time-independent weight of individual events in the likelihood analysis during the IC86b data period.

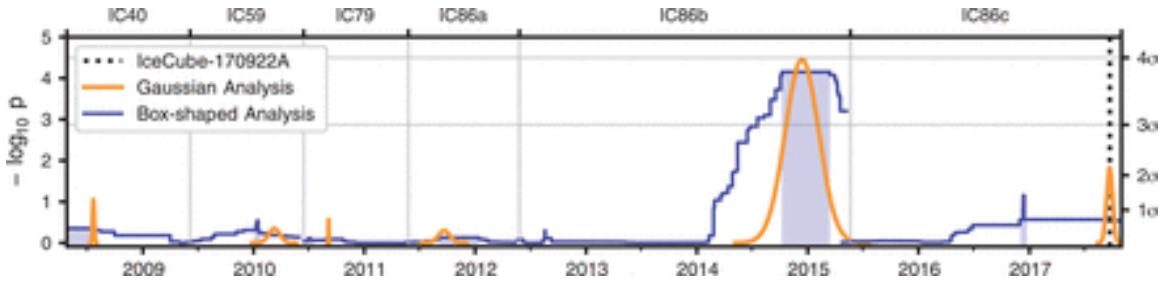

Fig. 1 Time-dependent analysis results.
The orange curve corresponds to the analysis using the Gaussian-shaped time profile. The central time T0 and width TW are plotted for the most significant excess found in each period, with the P value of that result indicated by the height of the peak. The blue curve corresponds to the analysis using the box-shaped time profile. The curve traces the outer edge of the superposition of the best-fitting time windows (durations TW) over all times T0, with the height indicating the significance of that window. In each period, the most significant time window forms a plateau, shaded in blue. The large blue band centered near 2015 represents the best-fitting 158-day time window found using the box-shaped time profile. The vertical dotted line in IC86c indicates the time of the IceCube-170922A event.

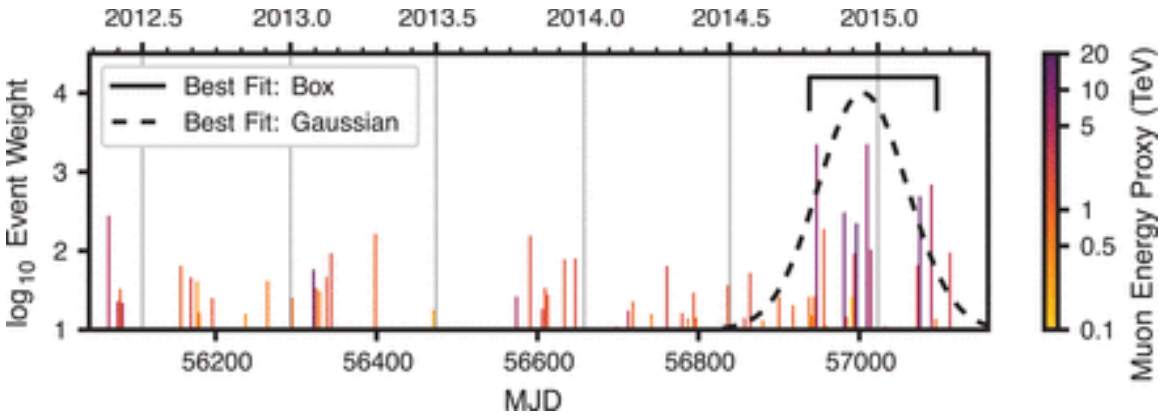

Fig. 2 Time-independent weight of individual events during the IC86b period.
Each vertical line represents an event observed at the time indicated by calendar year (top) or MJD (bottom). Overlapping lines are shifted by 1 to 2 days for visibility. The height of each line indicates the event weight: the product of the event's spatial term and energy term in the unbinned likelihood analysis evaluated at the location of TXS 0506+056 and assuming the best-fitting spectral index γ = 2.1 (*30*). The color for each event indicates an approximate value in units of TeV of the reconstructed muon energy (muon energy proxy), which the analysis compares with expected muon energy distributions under different hypotheses. [A distribution for the true neutrino energy of a single event can also be inferred from the event's muon energy (*30*).] The dashed curve and the solid bracket indicate the best-fitting Gaussian and box-shaped time windows, respectively. The distribution of event weights and times outside of the best-fitting time windows is compatible with background.

The Gaussian time window is centered at 13 December 2014 [modified Julian day (MJD) 57004] with an uncertainty of ±21 days and a duration $T_W = 110^{+35}_{-21}$ days. The best-fitting parameters for the fluence $J_{100} = \int \Phi_{100}(t)dt$ and the spectral index are given by $E^2J_{100} = 2.1^{+0.9}_{-0.7} \times 10^{-4}$ TeV cm^{-2} at 100 TeV and γ = 2.1 ± 0.2, respectively. The joint uncertainty on these parameters is shown in Fig. 3 along with a skymap showing the result of the time-dependent analysis performed at the location of TXS 0506+056 and in its vicinity during the IC86b data period.

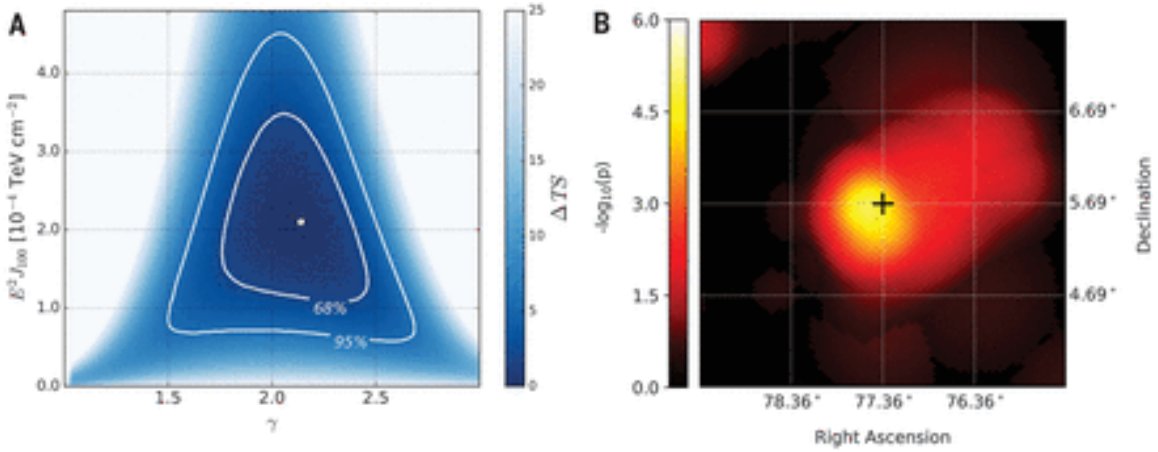

Fig. 3 Time-dependent analysis results for the IC86b data period (2012–2015).
(**A**) Change in test statistic, Δ*TS*, as a function of the spectral index parameter γ and the fluence at 100 TeV given by E^2J_{100}. The analysis is performed at the coordinates of TXS 0506+056, using the Gaussian-shaped time window and holding the time parameters fixed (T_0 = 13 December 2014, T_W = 110 days). The white dot indicates the best-fitting values. The contours at 68% and 95% confidence level assuming Wilks' theorem (*36*) are shown in order to indicate the statistical uncertainty on the parameter estimates. Systematic uncertainties are not included. (**B**) Skymap showing the *P* value of the time-dependent analysis performed at the coordinates of TXS 0506+056 (cross) and at surrounding locations. The analysis is performed on the IC86b data period, using the Gaussian-shaped time window. At each point, the full fit for (Φ, γ, T_0, T_W) is performed. The